Anthracene as a Launchpad for a Phosphinidene Sulfide and for Generation of a Phosphorus–Sulfur Material having the Composition P_2S, a Vulcanized Red Phosphorus that is Yellow

Wesley J. Transue,[†] Matthew Nava,[†] Maxwell W. Terban,[‡] Jing Yang,[¶] Matthew W. Greenberg,[§] Gang Wu,[‖] Elizabeth S. Foreman,[†] Chantal L. Mustoe,[⊥] Pierre Kennepohl,[⊥] Jonathan S. Owen,[§] Simon J. L. Billinge,[#,@] Heather J. Kulik,[¶] and Christopher C. Cummins*[,†]

†*Department of Chemistry, Massachusetts Institute of Technology, Cambridge, MA 02139, USA*
‡*Max Planck Institute for Solid State Research, Stuttgart, 70569, Germany*
¶*Department of Chemical Engineering, Massachusetts Institute of Technology, Cambridge, MA 02139, USA*
§*Department of Chemistry, Columbia University, New York, NY 10027, USA*
‖*Department of Chemistry, Queen's University, Kingston, ON K7L3N6, Canada*
⊥*Chemistry Department, University of British Columbia, Vancouver, BC V6T1Z1, Canada*
#*Department of Applied Physics & Applied Mathematics, Columbia University, New York, NY 10027, USA*
@*Condensed Matter Physics and Materials Science Department, Brookhaven National Laboratory, Upton, NY 11973, USA*

Received November 27, 2018; E-mail: ccummins@mit.edu

Abstract: Thermolysis of a pair of dibenzo-7-phosphanorbornadiene compounds is shown to lead to differing behaviors: phosphinidene sulfide release and formation of amorphous P_2S. These compounds, ^{t}BuP(S)**A** (**1**, **A** = $C_{14}H_{10}$ or anthracene; 59% isol. yield) and HP(S)**A** (**2**; 63%), are available through thionation of ^{t}BuP**A** and the new secondary phosphine HP**A** (**5**), prepared from Me_2NP**A** and DIBAL-H in 50% yield. Phosphinidene sulfide [^{t}BuP=S] transfer is shown to proceed efficiently from **1** to 1,3-dimethyl-2,3-butadiene to form Diels–Alder product **3** with a zero order dependence on diene. Platinum complex $(Ph_3P)_2Pt(\eta^2$-^{t}BuPS) (**4**, 47%) is also accessed from **1** and structurally characterized. In contrast, heating parent species **2** (3 h, 135 °C) under vacuum instead produces an insoluble, nonvolatile yellow residual material **6** of composition P_2S that displays semiconductor properties with an optical band gap of 2.4 eV. Material **6** obtained in this manner from molecular precursor **2** is in a poorly characterized portion of the phosphorus–sulfur phase diagram, and has therefore been subjected to a range of spectroscopic techniques to gain structural insight. X-ray spectroscopic and diffraction techniques, including Raman, XANES, EXAFS, and PDF, reveal **6** to have similarities with related compounds including P_4S_3, Hittorf's violet phosphorus. Various possible structures have been explored as well using quantum chemical calculations under the constraint that each phosphorus atom is trivalent with no terminal sulfide groups, and each sulfur atom is divalent. The structural conclusions are supported by data from phosphorus-31 magic angle spinning (MAS) solid state NMR spectroscopy, bolstering the structural comparisons to other phosphorus-sulfur systems while excluding the formulation of P_2S as a simple mixture of P_4S_3 and phosphorus.

1 Introduction

Anthracene-based molecular precursors have proven effective at delivering access to a range of reactive main group small molecules, including silylenes,[1] germylenes,[2] nitrous oxide,[3] phosphinidenes,[4,5] phosphaalkynes,[6] and sulfur monoxide,[7] among others.[8–11] These reactive fragments supported atop anthracene can often be extruded upon heating in a process driven by arene rearomatization. In pursuit of expanding the classes of small molecules accessible using this strategy, we have targeted the development of anthracene-based molecular precursors to phosphinidene sulfides ("thioxophosphines"). Phosphinidene sulfides have drawn recent interest as carbene analogs;[12–14] yet, their study is complicated by their general instability[15,16] and they are normally not isolated but rather generated *in situ*.[13,14,17,18] As such, molecular precursor chemistry stands to greatly assist our understanding of the chemistry of phosphinidene sulfides.

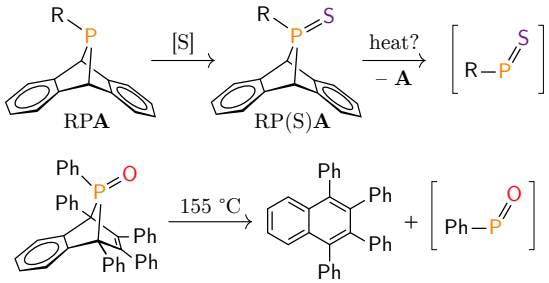

Scheme 1. Thionation of an RP**A** compound was envisioned to produce a molecular precursor for thermal release of a phosphinidene sulfide (RP=S) species (*top*), by analogy with Stille's classic phenylphosphinidene oxide precursor (*bottom*).[19]

Our previous studies on phosphinidene generation have shown that a phosphorus bridge can be installed across the 9,10-positions of anthracene in one step from several commercially available dichlorophosphines, $RPCl_2$, to yield RP**A** compounds (**A** = $C_{14}H_{10}$ or anthracene).[4,5] Addition of a sulfur atom to the phosphorus lone pair of RP**A** compounds was expected to yield RP(S)**A** compounds (Scheme 1), anthracene analogs of Stille's classic phenylphosphinidene oxide precursor.[19] Over the course of our studies, we have investigated two RP(S)**A** compounds, ^{t}BuP(S)**A** (**1**) and HP(S)**A** (**2**), and uncovered two disparate thermal fragmentation patterns. Behavior consistent with the anticipated phosphinidene sulfide release was observed for **1**, but **2** instead produced a new phosphorus–sulfur material, P_2S, upon heating. As effectively a form of "vulcanized red phosphorus," this material exists in a dis-

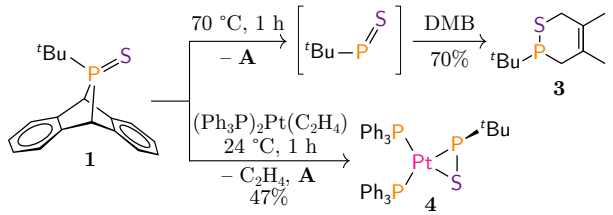

Scheme 2. Transfer from **1** can happen through free ^{t}BuP=S evolution at elevated temperatures, demonstrated by Diels–Alder cycloaddition with 2,3-dimethyl-1,3-butadiene (DMB), or through associative transfer as with $(Ph_3P)_2Pt(\eta^2\text{-}C_2H_4)$.

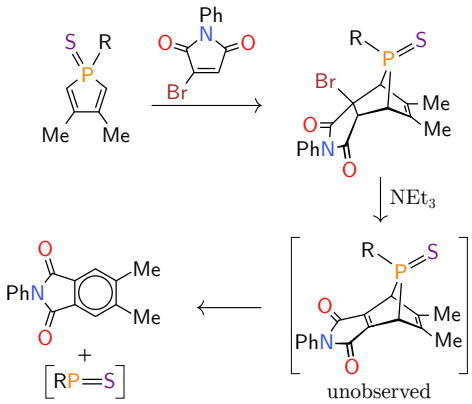

Scheme 3. A recent report of Wang and Mathey described a series of related precursors that likely fragment through an unobserved 7-phosphanorbornadiene intermediate.[12]

tinct and poorly characterized portion of the phosphorus–sulfur phase diagram, and is distinct from previously described "P_4S_2."[20–23]

2 Results & Discussion

2.1 Synthesis and Reactivity of ^{t}BuP(S)A

Our studies began by thionation of ^{t}BuP**A**[4] with $Ph_3As{=}S$,[24] providing ^{t}BuP(S)**A** (**1**) in 59% isolated yield. Thermal fragmentation at 70 °C with 2,3-dimethyl-1,3-butadiene (DMB) in benzene-d_6 solution gave quantitative anthracene formation and 70% conversion to Diels–Alder product **3** (Scheme 2).[12] Monitoring the kinetic profile of this process with NMR spectroscopy revealed a first-order dependence on the concentration of **1** that was independent of the concentration of DMB. This is consistent with rate limiting fragmentation of **1** into ^{t}BuP=S and anthracene followed by rapid interception by DMB, behavior analogous to that exhibited by related R$_2$NP**A** compounds.[5] An Eyring analysis allowed measurement of the activation barrier to be $\Delta H^{\ddagger}$ = 27.8(8) kcal/mol and $\Delta S^{\ddagger}$ = 8.0(2.4) cal/mol·K (Figure S.40), and density functional theory (DFT) calculations[25,26] at the RI-B2PLYP-D3(BJ)/Def2-TZVP level of theory[27–29] suggested fragmentation proceeds through concerted, asymmetric cheletropic cycloelimination (Figure 1). This pathway along the closed-shell singlet manifold was selected in comparison with other anthracene-based precursors,[5] but other fragmentation pathways including singlet and triplet biradical intermediates can also be envisioned.

This thermal fragmentation is quite similar to that from a recent report from Wang and Mathey.[12] Dehydrohalogenation of a precursor using triethylamine likely produced a 7-phosphanorbornadiene intermediate (Scheme 3); however,

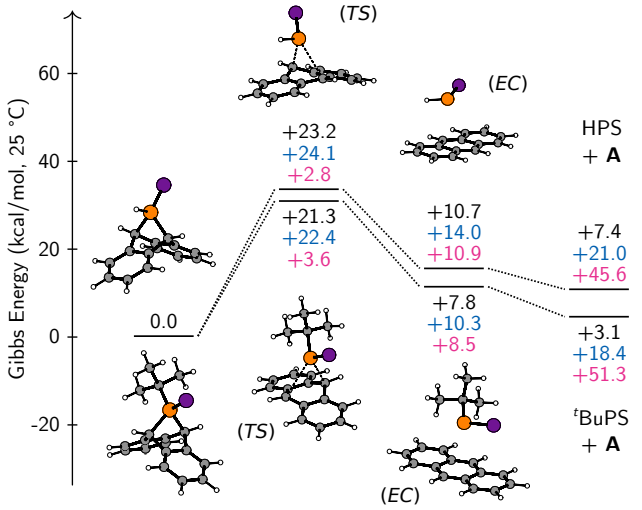

Figure 1. The predicted mechanisms for fragmentation of **1** and **2** at the RI-B2PLYP-D3(BJ)/Def2-TZVP level of theory, involving an asymmetric transition state (*TS*) and an encounter complex (*EC*). The Gibbs free energy (kcal/mol, 25 °C, black) is shown along with enthalpy (kcal/mol, blue) and entropy (cal/mol·K, pink).

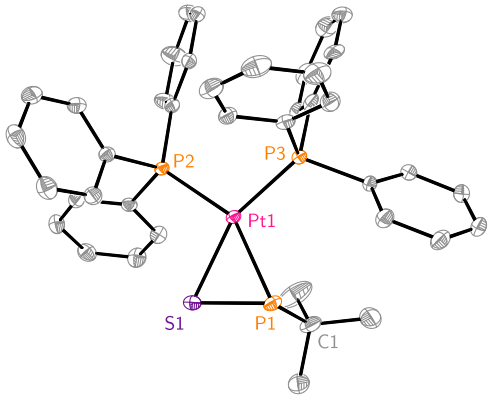

Figure 2. Structure of **4** from an X-ray diffraction study shown with 50% probability thermal ellipsoids. Hydrogen atoms and a solvent of crystallization have been omitted for clarity. Selected interatomic distances [Å] and angles [°]: Pt1–P1 2.3689(13), Pt1–S1 2.3490(13), P1–S1 2.0678(19), Pt1–P2 2.3148(12), Pt1–P3 2.2550(13); P1–Pt1–S1 51.99(5), Pt1–S1–P1 64.50(5), S1–P1–Pt1 63.51(5), S1–P1–C1 104.4(2).

this intermediate was not observed and was described to immediately collapse. Depending on the substituent, this transformation was performed at either room temperature or 110 °C to produce the phthalimide and transfer [RP=S] to DMB.

In addition to the proposed thermal generation of free ^{t}BuP=S, **1** was also competent at ^{t}BuP=S transfer without thermal activation, behavior consistent with an associative process. Treatment with $(Ph_3P)_2Pt(\eta^2\text{-}C_2H_4)$ in DCM solution resulted in a rapid reaction at 22 °C, producing $(Ph_3P)_2Pt(\eta^2\text{-}^t\text{BuP=S})$ (**4**) along with ethylene and anthracene. Complex **4** was isolated in 47% yield by fractional recrystallization from diethyl ether. To the best of our knowledge, this phosphinidene sulfide complex is the first reported for a group 10 metal. A wide variety of synthetic methods for RP=S assembly at a transition metal have been reported, including reduction of RP(S)Cl$_2$ compounds,,[30] interception of free RP=S species,[31] deprotonation of thiophosphine complexes,[32] thionation of phos-

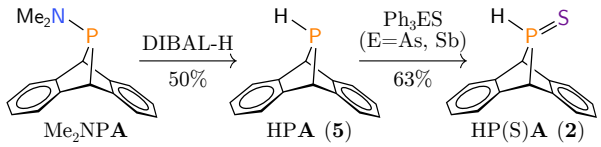

Scheme 4. Preparation of molecular precursor **2** proceeded in two steps from Me_2NP**A**.

phinidene complexes,[33,34] and unselective reactions with Lawesson's reagent,[35] among others.[36] An X-ray crystallographic study (Figure 2) revealed a P···S interatomic distance of 2.068(2) Å, intermediate between standard single P–S (2.14 Å) and double P=S (1.96 Å) bond lengths,[37] indicating significant back-donation by the platinum center. Analysis of model complex $(Me_3P)_2Pt(\eta^2$-MeP=S) by natural bond orbital (NBO)[38] methods revealed a P–S natural bond order of 1.2, a Pt–P bond order of 0.4, a Pt–S bond order of 0.4, a platinum natural charge of 0.0, and a platinum natural electron configuration of $[Xe]6s^{0.7}5d^{9.3}$. These results suggest **4** to be somewhat closer to a platinum(0) complex than a platinum(II) complex; however, the square planar geometry and natural bond orders clearly show a high degree of platinum(II) character.

2.2 Synthesis of HPA (5) and HP(S)A (2)

As a precursor to ^{t}BuP=S, **1** exhibits several desirable features over many previously reported precursors.[18] It does not require exogenous base[12] or reductant,[30,39] and it can be activated thermally rather than photochemically.[40,41] We were therefore excited to investigate whether this platform could be used to access the parent phosphinidene sulfide, HP=S, also known as "thioxophosphane." This second-row analog of HN=O is stable in the gas phase[42] and has been proposed to be a species of astrochemical importance,[43,44] but has only been lightly studied following its unselective production by high energy electric discharge and ionization methods.[42,44,45]

Synthesis of parent secondary phosphine sulfide HP(S)**A** (**2**) required HP**A** (**5**) as an intermediate. Though successful for other strained chlorophosphines,[46] we found reduction of ClP**A** with $LiAlH_4$ and similar nucleophilic hydride sources to give only decomposition, likely due to the fragility of the strained C–P–C bridge towards nucleophilic opening *à la* aziridines and phosphiranes.[47,48] Instead, treatment of Me_2NP**A** with an electrophilic hydride source, di-*iso*-butylaluminum hydride (DIBAL-H, 2.2 equiv.), in thawing toluene provided **5** (^{31}P δ 162 ppm, $^1J_{PH}$ = 161 Hz) in fair yield (50%, Scheme 4).[49] A single crystal X-ray diffraction study revealed structural parameters in line with those reported for other RP**A** species (Figure 3*a*). This light-sensitive compound was not found to fragment thermally into anthracene and phosphinidene HP̈: upon heating, in agreement with our current understanding of requisite substituent patterns for phosphinidene generation.[5,50]

Thionation of **5** proceeded cleanly in THF solution using Ph_3E=S (E = As, Sb), the resultant **2** precipitating directly (Scheme 4). Collection by filtration and washing with diethyl ether provided clean **2** in 63% yield (^{31}P δ 118 ppm, $^1J_{PH}$ = 456 Hz). The strong $^1J_{PH}$ coupling clarified **2** to exist as the secondary phosphine sulfide tautomer rather than thiophosphinous acid HS–P**A**. Such a tautomer would also be an interesting compound as a possible precursor to HSP,[51] another species known to be stable in the gas phase.[42] Unexpectedly poor solubility properties were observed in many common organic solvents including benzene, diethyl ether, THF, and hexane, but **2** is soluble in the more polar solvents acetonitrile, dichloromethane, and pyridine. X-ray crystallographic characterization revealed extended hydrogen-bonding chains of **2** (Figures 3*b* and 4), explaining the poor solubility in solvents that do not readily engage in hydrogen bonding.

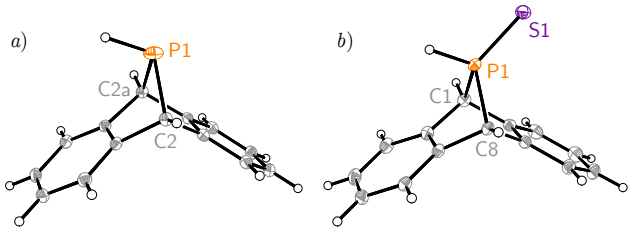

Figure 3. Structures of (*a*) **5** and (*b*) **2** from single-crystal X-ray diffraction studies shown with 50% probability thermal ellipsoids. (*a*) Selected interatomic distances [Å] and angles [°] for **5**: P1–C2 1.900(2); C2–P1–C2a 79.51(13). (*b*) Selected interatomic distances [Å] and angles [°] for **2**: P1–C1 1.8766(17), P1–C8 1.8716(18), P1–S1 1.9414(7); C1–P1–C8 82.40(8), C1–P1–S1 121.53(6), C8–P1–S1 121.87(6).

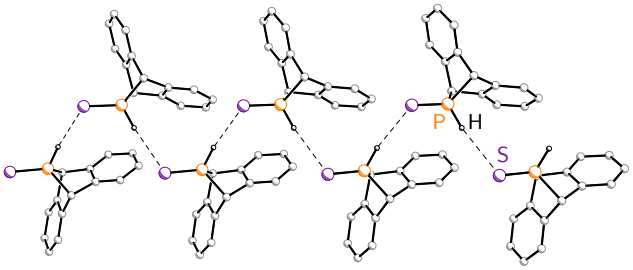

Figure 4. A depiction of the hydrogen bonding network of **2** in the crystal. Selected interatomic distance [Å] and angles [°]: P–H 1.35(2), H–S 2.99(2), P–S 4.3033(7); P–H–S 166(1).

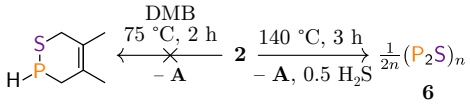

Scheme 5. Thermal fragmentation of **2** does not give competent HP=S transfer to 2,3-dimethyl-1,3-butadiene (DMB), instead yielding a solid yellow P_2S (**6**) material.

2.3 Formation of an Amorphous P_2S Material

Thermal fragmentation of **2** into anthracene and transient [HP=S] was anticipated in analogy to the behavior of **1**. Computational studies supported this expectation, predicting an activation barrier only $\Delta\Delta G^{\ddagger}$ = 1.9 kcal/mol higher than that of **1** (Figure 1). However, heating a pyridine solution of **2** in the presence of DMB to 75 °C for 2 h did not yield the expected Diels-Alder product, instead giving a yellow insoluble precipitate (**6**) and quantitative production of anthracene (Scheme 5). Yellow insoluble solids were also observed upon heating **2** in solutions lacking DMB and when heating the solid compound under vacuum.

To probe for the presence of [HP=S] in the gaseous effluent from heating solid **2**, we turned to molecular beam mass spectrometry (MBMS). At a temperature of *ca.* 100 °C, we observed release of a fragment at 34 m/z rather than 64 m/z ($HP{=}S^+$). This could correspond to either PH_3^+ or H_2S^+. Definitive identification was accomplished by condensation

of the gas into an NMR tube that was then flame sealed and analyzed by ^{1}H and ^{31}P NMR spectroscopy, showing release of H_2S with only traces of PH_3.

The yellow insoluble material **6** was accessed more straightforwardly by heating solid **2** within a sublimation apparatus to 130–140 °C under vacuum ($\sim 10^{-5}$ torr) for 3 h, allowing nearly quantitative anthracene recovery on the cold finger. The yellow waxy solid so obtained is insoluble in common organic solvents, including acetone, THF, diethyl ether, benzene, hexane, chloroform, and carbon disulfide. It was found to undergo reactive dissolution in DMSO to yield several phosphorus(V) species (SI §S.1.7). The reaction of **6** with DMSO indicates that this is a reduced material capable of oxygen atom abstraction from DMSO. The presence of several species is reminiscent of the known nonselective reactivity of DMSO with phosphorus(V) oxides.[52]

Elemental analysis revealed for **6** a phosphorus-to-sulfur ratio of 68:32, corresponding to a species of approximate composition P_2S, and energy-dispersive X-ray (EDX) spectroscopy showed a uniform distribution of these elements at this same ratio. Minimal organic contaminants remained (<5%) that were found by magic angle spinning (MAS) solid-state NMR (SSNMR) studies to comprise primarily anthracene and **2**. With these data, we concluded that the material has a polymeric structure, as no stable molecular species with a P_2S empirical formula are known and any such material should exhibit higher solubility in organic solvents.[53,54] The mechanism of formation of **6** remains unclear, but the hydrogen bonding network in the crystal structure of solid **2** suggests initial condensation (2 **2** → H_2S + $S(P\mathbf{A})_2$) and subsequent anthracene release. At the present time, direct reaction of two HPS molecules to form H_2S and transient [P_2S] cannot be excluded.[55]

The thermodynamic properties of phosphorus sulfides that define the phase diagram are complicated,[56] and the particular portion of the phosphorus–sulfur binary phase diagram around P_2S is poorly understood:[57–60] there are only four reports of the phase diagram that discuss "P_4S_2." Two initial reports by Förthmann and Schneider[20,21,61] characterized "P_4S_2" as a low-melting (46–49 °C) solid. Subsequent work by Vincent and Vincent-Forat[22,23] disputed this, claiming P_4S_2 to be available only through peritectic reaction between P_4S_3 and liquid phosphorus-sulfur below –30 °C. Our P_2S material **6**, a canary yellow solid prepared at 130 °C, clearly matches neither description. Continued heating was found to prompt melting with decomposition at 170 °C, implying metastability akin to previously reported P_4S_2 due to other P_xS_y phases lying thermodynamically downhill.[62] Although **6** was insoluble in CS_2, extraction with CS_2 of resolidified **6** after melting at 185 °C showed both P_4S_3 and P_4 in a roughly 6:1 ratio (*ca.* 2:1.2 P–S ratio) with some residual insoluble red–brown material, emphasizing the metastability of **6** as a thermodynamically uphill phase from P_4S_3, P_4, and red phosphorus.

2.4 Spectroscopic Characterization of P_2S

Unlike Vincent's report of low-temperature powder X-ray diffraction (PXRD) studies of traditional P_4S_2,[23] PXRD of this new P_2S material revealed only two broad features at $2\theta = 31°$ and 16° (Figure S.47). Such features are characteristic of an amorphous material with only short-range order. Lack of extended periodicity necessarily limited precise structural description for the material; nonetheless, there is a long history of structural investigations of amorphous solids and glasses. In pursuit of some degree of structural elucidation, we have submitted P_2S to a battery of spectroscopic characterization techniques.

Raman vibrational spectroscopy has not revealed the presence of P–H, S–H, or P=S bonds,[63–65] consistent with release of H_2S during thermolysis of **2** (Figure 5). Neither anthracene nor **2** was present in detectable amounts, showing a high degree of conversion to P_2S. The lack of P=S stretches is consistent with the presence of reduced phosphorus centers as expected from the reductive reactivity observed with DMSO. The similar masses of phosphorus and sulfur limit further interpretation of the Raman spectrum; however, the observed bands (200–500 cm^{-1}) are in the expected region by comparison with other phosphorus-sulfur compounds,[66] red phosphorus,[67] and phosphorus-sulfur glasses.[68]

^{31}P MAS SSNMR spectroscopy allowed direct interrogation of the range of phosphorus nuclear environments within the solid (Figure 6). The spectra were fit as a linear combination of four sites with center bands ranging from δ_{iso} = 35–150 ppm (Table 1); however, it should be noted that the signal-to-noise and broad features reduced the reliability of the simulated integrations. The large linewidths are symptomatic of nonuniform atomic environments inherent to amorphous materials.

The two most abundant peaks, sites 1 and 2, together account for a majority of the total simulated signal intensity, and exhibit ^{31}P chemical shift tensors (skew $\kappa < 0$) similar to those observed for P^{III}–S sites in phosphorus sulfides.[69] The small skew values ($|\kappa| < 0.5$) are suggestive of large variations in the S–P–S angles around the P^{III} centers. Site 4 is reminiscent of one of three signals observed in phosphorus-rich P–Se glasses that was tentatively assigned to a [P_4Se_2] unit as a P^{III} center bonded to two chalcogens and one phosphorus.[70] Evidence supporting a similar assignment in P_2S also came from comparison of site 4 with other molecular phosphorus sulfides.[71]

The signals for site 3 are sharper than the others, and it exhibits a similar chemical shift tensor to the apical phosphorus center of P_4S_3 and to the phosphorus centers of P_4Se_4.[71,72] The presence of P_4S_3 would be reasonable as it is a stable molecular species; however, a corresponding resonance for the basal centers was not detected. Despite

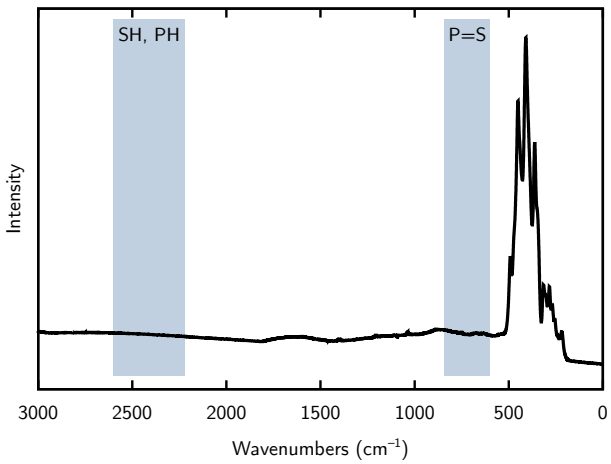

Figure 5. Raman spectrum (785 nm excitation) of the P_2S material with regions corresponding to P–H,[63] S–H,[64] and P=S[65] stretches highlighted.

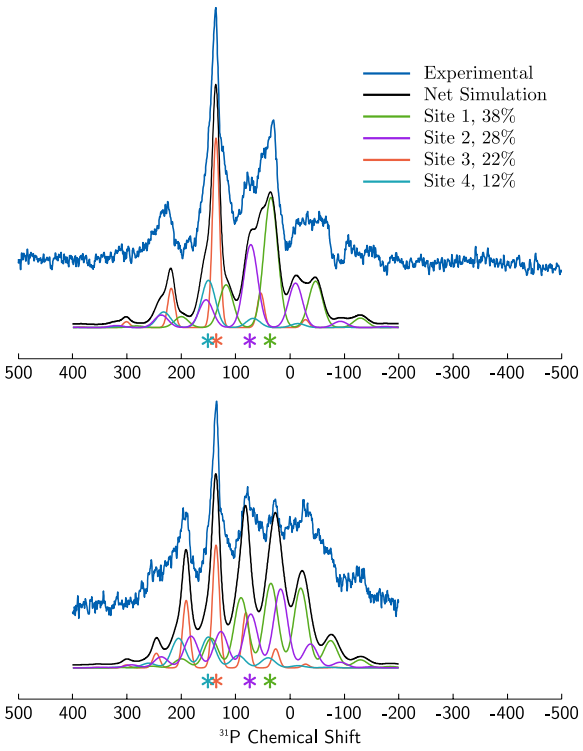

Figure 6. Experimental and simulated ^{31}P MAS SSNMR spectra of P_2S obtained at 21 T, 20 °C, and a spinning rate of (*top*) 30 kHz and (*bottom*) 20 kHz. Asterisks have been placed beneath the center band of each simulated site.

the generally wide and indistinct chemical shift range for phosphorus–sulfur species,[73] chemical shifts in the upfield region of δ –60 to –100 ppm are indicative of three-membered rings.[70,74] As none of the simulated sites display an isotropic shift in this region, we can reasonably exclude *cyclo*-$P_{3-x}S_x$ units as major structural components of the P_2S material. This suggests P_2S is not a simple mixture of P_4S_3 and phosphorus, and the lack of P_4S_3 was additionally supported by its absence upon dissolution of P_2S in DMSO-d_6 as analyzed by solution ^{31}P NMR spectroscopy (SI §S.1.7).

X-ray photoemission spectroscopy (XPS) provided insight into the oxidation states of the phosphorus and sulfur centers (Figure 7*a*,*c*). The phosphorus 2*p* binding energies of P_2S (primarily 131.1 eV) revealed reduced phosphorus centers by comparison with relevant literature species: red phosphorus (129.9–130.1 eV), P_4S_3 (130.5 eV), P_4S_5 (132.0, 134.9 eV), P_4S_7 (132.7, 134.3 eV).[75–77] The sulfur 2*p* binding energies (163.0 eV, 164.1 eV) observed for **6** are similar to that of S_8 (163.8 eV).[78] Oxidation states near zero for both phosphorus and sulfur match well with our understanding from the other spectroscopies.

Table 1. Fitting parameters for the ^{31}P MAS SSNMR spectrum of P_2S (**6**) and HP(S)**A** (**2**) at 21 T

Site	δ_{iso}	δ_{11}	δ_{22}	δ_{33}	Ω^a	κ^b
1, 38%	35	185	27	–107	292	–0.08
2, 28%	72	252	27	–63	315	–0.43
3, 22%	136	244	148	16	228	0.16
4, 12%	150	240	210	0	240	0.75
2	115.7	243.7	102.7	0.7	243	–0.16

[a] Span $\Omega = \delta_{11} - \delta_{33}$ [b] Skew $\kappa = 3(\delta_{22} - \delta_{iso})/\Omega$

X-ray absorption near-edge spectroscopy (XANES) corroborated the XPS analysis (Figure 7*b*,*d*). The phosphorus K-edge feature observed at 2145 eV is similar to that for red phosphorus at 2144.5 eV.[79] Similarly, the sulfur K-edge feature at 2471 eV is more similar to that of S_8 (2472.7 eV) than to corresponding values for organosulfur compounds (e.g., dibenzothiophene 2474.0 eV).[80] Poor quality *k*-space scattering data limited the accuracy with which the fine structure could be interpreted from the extended region (EXAFS, SI Figure S.54). Both phosphorus and sulfur *R*-space distributions showed a nearby scatterer at ∼2.0 Å, an appropriate distance for P–P, P–S, and S–S bonds.[37] The higher-quality sulfur trace showed additional scatterers in the 3–4 Å range, as expected from the next nearest neighbor.

The X-ray pair distribution function (PDF)[83] provided higher resolution data than EXAFS, allowing more precise structural commentary (Figure 8). The PDF signal indicated an approximate measure of the average coherently scattering domain size to be 20–30 Å by observation of the distance at which peaks are no longer resolvable. Such a small domain size is consistent with the amorphous, nonperiodic nature of the P_2S material.

The PDF data for **6** exhibit many shared features with simulated data for other phosphorus-rich P_xS_y compounds, P_xSe_y compounds, and with several phosphorus allotropes (Figure 9, SI §S.5.7). The most prominent features are at 2.16 and 3.40 Å, in the expected range for first- and second-nearest neighbor P–P, P–S, and S–S interatomic distances.[37] There is good agreement with data for P_4S_3 at short distances, indicating similar bonding environments between the materials in the first- and second-nearest neighbor region. There is additionally moderate agreement in the 4–8 Å range, suggesting similarity in the packing of molecular subunits (Figure 10). At larger distances, none of the known P_xS_y, P_xSe_y, or phosphorus allotropes matches well with the PDF data for **6**, highlighting the unique structure of the material. Maximal agreement was achieved by refining separate intra- and intermolecular thermal parameters, and with addition of a damping function to reduce the distance-wise structural coherence.

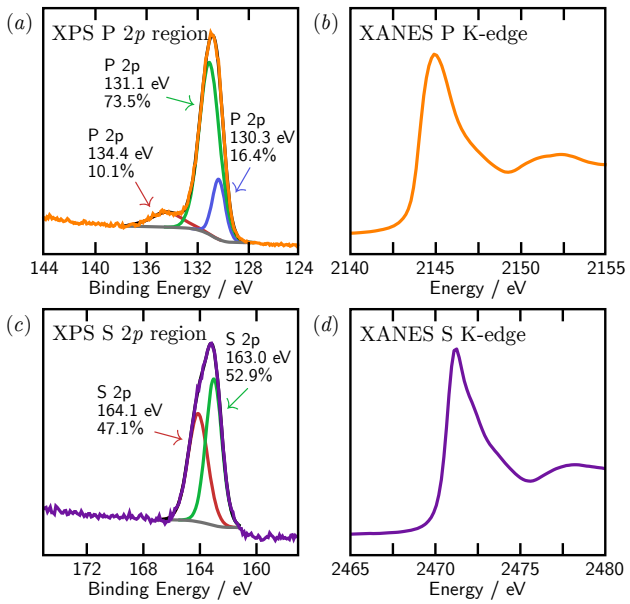

Figure 7. XPS (*a*, *c*) and XANES (*b*, *d*) analyses of the phosphorus (*a*, *b*) and sulfur (*c*, *d*) centers of P_2S.

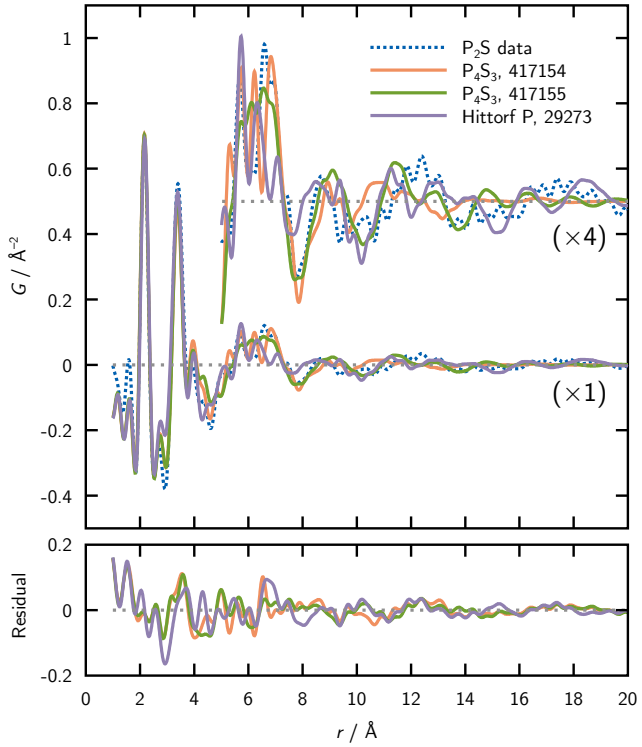

Figure 8. The PDF data acquired on P_2S plotted alongside simulated PDF data for two crystal structures of P_4S_3 with ICSD codes 417154 and 417155 and of Hittorf's violet phosphorus with ICSD code 29273.[81,82] Magnification (×4) of the $r > 5$ Å region reveals additional features of the P_2S data not reproduced by P_4S_3 or Hittorf's violet phosphorus.

The EXAFS and PDF features observed for **6** are reminiscent of the data acquired on vitreous P_2Se, a relevant phosphorus–selenium amorphous glass that has been known for several decades and is accessed by heating elemental P and Se.[85–88] Through a combination of Raman, EXAFS, and neutron scattering experiments, Verrall *et al.* initially concluded that P_2Se is composed of P_4Se_3 cages with the basal *cyclo*-P_3 ring split by additional phosphorus to span neighboring units.[85] Later studies by both Verrall and others have also since demonstrated the presence of intact P_4Se_3 molecules by EXAFS, Raman, and ^{31}P MAS SSNMR spectroscopies.[70,86–88] The observed lack of significant P_4S_3 in P_2S shows there to be differences in structure between P_2S and P_2Se; however, the reported structure of P_2Se raises the possibility for **6** of relatively sulfur-rich clusters embedded within a phosphorus-rich matrix.[89,90]

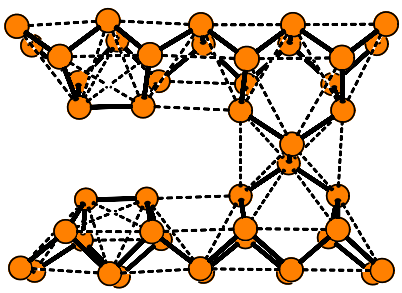

Figure 9. At short distances ($\lesssim$4 Å), most phosphorus allotropes and phosphorus-rich P_xS_y compounds have strong similarities with P_2S, illustrated here with several interatomic distances of Hittorf's violet phosphorus that match the 2.15 (*solid*) and 3.35 Å (*dashed*) features of the P_2S PDF data.[82]

Similar to several studies of vitreous P_2Se,[89,90] we performed calculations on several candidate molecular and extended structures (SI §S.7.2). A wide variety of structures show fair agreement with the closest $r \lesssim 5$ Å region due to the similarity of P–P, P–S, and S–S interatomic distances; however, features at longer distances were difficult to reproduce. At these distances, agreement is influenced more strongly by packing effects than elemental composition, leading us to explore species with P_xS_y compositions deviating from $x = 2y$. Despite many attempts simulations of P_4S_3 still reproduce the 5–8 Å features best; however, optimization of the geometry of $[P_4S_4]_\infty$, an unknown sulfur analog of the known $[P_4Se_4]_\infty$,[84] gave fair agreement in the 10–20 Å region to the broad features, possibly indicating similar packing of clusters at these distances (Figure 11).

Together, our spectroscopic and diffraction data reveal P_2S to be composed likely of interconnected rings and bicyclic structures reminiscent of Hittorf's violet phosphorus and P_4S_3. Raman, XPS, XANES, and PDF data reveal reduced phosphorus centers lacking P=S bonds, and NMR analysis did not show the presence of three-membered rings. Clusterings of atoms appear to be spaced roughly analogously to P_4S_3 at around 5–7 Å with further clusters appearing on average at 12 and 17 Å sharing similarities with the calculated packing of $[P_4S_4]_\infty$ polymers.

Although high in phosphorus content and spectroscopically similar to red phosphorus, **6** is canary yellow and visually appears more similar to yellow sulfur than red phosphorus. Diffuse reflectance UV–Vis spectroscopy showed the onset of absorbance to lie at *ca.* 500 nm, and analysis with a Tauc plot allowed extrapolation of an optical indirect band gap of 2.38 eV (Figure S.57).[91] Initial pressed-pellet conductivity measurements show a modest conductivity of 2.5×10^{-5} S/cm that is in line with the relatively large optical band gap. These data suggest that P_2S may behave as a group V–VI (15–16) wide band gap semiconductor. To the best of our knowledge, a phosphorus–sulfur semiconductor has not been reported and this result suggests that further P_xS_y materials may find semiconductor applications as heavier V–VI semiconductors have.[92]

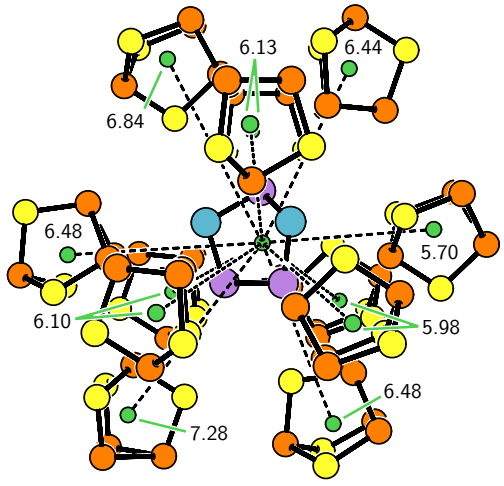

Figure 10. The agreement between the PDF data for P_4S_3 and P_2S in the 4–8 Å range indicates similar distances between adjacent units, here represented by the distances (Å) between centroids (green) of nearby P_4S_3 molecules (*central* purple–blue, *adjacent* orange–yellow) in the crystal lattice.[81]

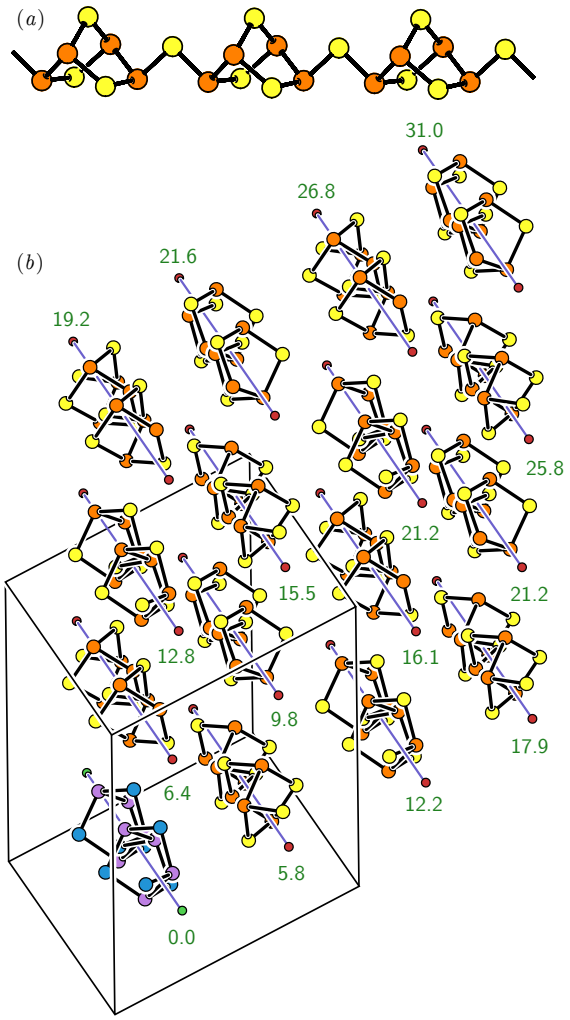

Figure 11. (*a*) *Ab initio* chain structure of $[P_4S_4]_\infty$ calculated from the known structure of $[P_4Se_4]_\infty$.[84] (*b*) Packing diagram of chains of $[P_4S_4]_\infty$ shown with the interchain distances (Å) to the blue–purple chain at the lower left, showing features clustered around 6, 9, 12, and 17 Å roughly agreeing with P_2S PDF data.

3 Conclusion

In summary, we have found two contrasting behaviors of RP(S)**A** molecules. Compound **1** has been demonstrated to be competent at transfer of ^{t}BuP=S under mild thermal conditions. Its participation in associative fragment transfer to a platinum(0) complex to generate the first group 10 phosphinidene sulfide complex also points towards further chemistry of phosphinidene sulfides available from anthracene-based precursors.

The observed intermolecular close association in the solid state structure of **2** is connected with the intermolecular reactivity upon heating leading to H_2S evolution rather than HP=S evolution. Molecular precursors to sterically unprotected reactive small molecules may need to be designed in such a way that they are prevented from engaging in close association and bimolecular reactivity in the solid state; they may need to be site isolated in order to evolve a molecule such as HPS into the gas phase.

The fragmentation of **2** to produce **6** hints at a broader applicability of anthracene-based molecular precursors in materials chemistry.[93] The production of anthracene as a volatile byproduct suggests that molecules such as **2** may hold particular promise as precursors in chemical vapor deposition or thin film formation studies. The particular material attained from **2** in this study is of additional interest due to its unusual ratio of elements. Our spectroscopic and diffraction studies have shown that its average structure has many similarities with those of P_4S_3 and Hittorf's violet phosphorus. It is noteworthy that red phosphorus has recently been used as a photocatalyst in the hydrogen evolution reaction,[94] and new main group materials like **6** may find similar applications. The preparation of **6** also renews questions about this phosphorus-rich portion of the phosphorus–sulfur phase diagram.

Acknowledgement This material is based on research supported by the National Science Foundation under CHE-1664799 and ECCS-1449291. PDF data collection and analysis in the Billinge group was supported by the NSF MRSEC program through Columbia in the Center for Precision Assembly of Superstratic and Superatomic Solids (DMR-1420634). X-ray PDF measurements were conducted on beamline 28-ID-2 of the National Synchrotron Light Source II, a U.S. Department of Energy (DOE) Office of Science User Facility operated for the DOE Office of Science by Brookhaven National Laboratory under Contract No. DE-SC0012704. MWT acknowledges support from BASF. GW thanks NSERC of Canada for funding. HJK holds a Career Award at the Scientific Interface from the Burroughs Wellcome Fund. Use of the Stanford Synchrotron Radiation Lightsource, SLAC National Accelerator Laboratory, is supported by the U.S. Department of Energy, Office of Science, Office of Basic Energy Sciences under Contract No. DE-AC02-76SF00515. The SSRL Structural Molecular Biology Program is supported by the DOE Office of Biological and Environmental Research, and by the National Institutes of Health, National Institute of General Medical Sciences (including P41GM103393). The contents of this publication are solely the responsibility of the authors and do not necessarily represent the official views of NIGMS or NIH. We gratefully acknowledge Maciej D. Korzyński, Grigorii Skorupskii, Lilia S. Xie, and Martin-Louis Riu for assistance in data acquisition.

Supporting Information Available Experimental details, characterization data, and X-ray crystallographic information are provided in the Supporting Information document.

References

(1) Mayer, B.; Neumann, W. P. 7-Silanorbornadienes and their thermal cycloeliminations. *Tetrahedron Lett.* **1980**, *21*, 4887–4890.
(2) Velian, A.; Transue, W. J.; Cummins, C. C. Synthesis, Characterization, and Thermolysis of Dibenzo-7-dimethylgermanorbornadiene. *Organometallics* **2015**, *34*, 4644–4646.
(3) Carpino, L. A.; Padykula, R. E.; Barr, D. E.; Hall, F. H.; Krause, J. G.; Dufresne, R. F.; Thoman, C. J. Synthesis, characterization, and thermolysis of 7-amino-7-azabenzonorbornadienes. *J. Org. Chem.* **1988**, *53*, 2565–2572.
(4) Velian, A.; Cummins, C. C. Facile Synthesis of Dibenzo-7λ^3-phosphanorbornadiene Derivatives Using Magnesium Anthracene. *J. Am. Chem. Soc.* **2012**, *134*, 13978–13981.
(5) Transue, W. J.; Velian, A.; Nava, M.; García-Iriepa, C.; Temprado, M.; Cummins, C. C. Mechanism and Scope of Phosphinidene Transfer from Dibenzo-7-phosphanorbornadiene Compounds. *J. Am. Chem. Soc.* **2017**, *139*, 10822–10831.
(6) Transue, W. J.; Velian, A.; Nava, M.; Martin-Drumel, M.-A.; Womack, C. C.; Jiang, J.; Hou, G.-L.; Wang, X.-B.; McCarthy, M. C.; Field, R. W.; Cummins, C. C. A Molecular Precursor to Phosphaethyne and Its Application in Synthesis of the

Aromatic 1,2,3,4-Phosphatriazolate Anion. *J. Am. Chem. Soc.* **2016**, *138*, 6731–6734.
(7) Joost, M.; Nava, M.; Transue, W. J.; Martin-Drumel, M.-A.; McCarthy, M. C.; Patterson, D.; Cummins, C. C. Sulfur monoxide thermal release from an anthracene-based precursor, spectroscopic identification, and transfer reactivity. *Proc. Natl. Acad. Sci.* **2018**, *115*, 5866–5871.
(8) Velian, A.; Nava, M.; Temprado, M.; Zhou, Y.; Field, R. W.; Cummins, C. C. A Retro Diels–Alder Route to Diphosphorus Chemistry: Molecular Precursor Synthesis, Kinetics of P_2 Transfer to 1,3-Dienes, and Detection of P_2 by Molecular Beam Mass Spectrometry. *J. Am. Chem. Soc.* **2014**, *136*, 13586–13589.
(9) Courtemanche, M.-A.; Transue, W. J.; Cummins, C. C. Phosphinidene Reactivity of a Transient Vanadium PN Complex. *J. Am. Chem. Soc.* **2016**, *138*, 16220–16223.
(10) Joost, M.; Nava, M.; Transue, W. J.; Cummins, C. C. An exploding N-isocyanide reagent formally composed of anthracene, dinitrogen and a carbon atom. *Chem. Commun.* **2017**, *53*, 11500–11503.
(11) Joost, M.; Transue, W. J.; Cummins, C. Diazomethane umpolung atop anthracene: An electrophilic methylene transfer reagent. *Chem. Sci.* **2018**, *9*, 1540–1543.
(12) Wang, L.; Ganguly, R.; Mathey, F. Revisiting the Chemistry of Phosphinidene Sulfides. *Organometallics* **2014**, *33*, 5614–5617.
(13) Graham, C. M. E.; Pritchard, T. E.; Boyle, P. D.; Valjus, J.; Tuononen, H. M.; Ragogna, P. J. Trapping Rare and Elusive Phosphinidene Chalcogenides. *Angew. Chem. Int. Ed.* **2017**, *56*, 6236–6240.
(14) Graham, C. M. E.; Macdonald, C. L. B.; Boyle, P. D.; Wisner, J. A.; Ragogna, P. J. Addressing the Nature of Phosphinidene Sulfides via the Synthesis of P-S Heterocycles. *Chem. Eur. J.* **2018**, *24*, 743–749.
(15) Jochem, G.; Karaghiosoff, K.; Plank, S.; Dick, S.; Schmidpeter, A. Ylidylphosphorsulfide, -selenide, -disulfide, -sulfidselenide und -diselenide. *Chem. Ber.* **1995**, *128*, 1207–1219.
(16) Yoshifuji, M.; Sangu, S.; Hirano, M.; Toyota, K. A Stabilized Phosphinothioylidene Generated by Deselenation of a Selenoxothioxophosphorane. *Chem. Lett.* **1993**, *22*, 1715–1718.
(17) Gaspar, P. P.; Beatty, A. M.; Li, X.; Qian, H.; Rath, N. P.; Watt, J. C. Phosphinidenes, Phosphiranes, and their Chalcogenides. *Phosphorus Sulfur Silicon Relat. Elem.* **1999**, *144*, 277–280.
(18) Gaspar, P. P.; Qian, H.; Beatty, A. M.; d'Avignon, D. A.; Kao, J. L. F.; Watt, J. C.; Rath, N. P. 2,6-Dimethoxyphenylphosphirane Oxide and Sulfide and their Thermolysis to Phosphinidene Chalcogenides—Kinetic and Mechanistic Studies. *Tetrahedron* **2000**, *56*, 105–119.
(19) Stille, J. K.; Eichelberger, J. L.; Higgins, J.; Freeburger, M. E. Phenylphosphinidene oxide. Thermal decomposition of 2,3-benzo-1,4,5,6,7-pentaphenyl-7-phosphabicyclo[2.2.1]hept-5-ene oxide. *J. Am. Chem. Soc.* **1972**, *94*, 4761–4763.
(20) Förthmann, R.; Schneider, A. Das System Schwefel–Phosphor. *Naturwissenschaften* **1965**, *52*, 390–391.
(21) Förthmann, R.; Schneider, A. Das System Schwefel-Phosphor. *Z. Physik. Chem.* **1966**, *49*, 22–37.
(22) Vincent, H. Diagramme de phases phosphore-soufre. *Bull. Soc. Chim. Fr.* **1972**, 4517–4521.
(23) Vincent, H.; Vincent-Forat, C. Étude des sulfures de phosphore P_4S_9–P_4S_4–P_4S_2. *Bull. Soc. Chim. Fr., Partie 1* **1973**, 499–502.
(24) Brown, D. H.; Cameron, A. F.; Cross, R. J.; McLaren, M. Preparation of tertiary arsine sulphides. Crystal and molecular structures of the adduct of $AsMePh_2S$ and $P(NMe_2)_3O$. *J. Chem. Soc., Dalton Trans.* **1981**, 1459–1462.
(25) Neese, F. The ORCA program system. *WIREs Comput. Mol. Sci.* **2012**, *2*, 73–78.
(26) Neese, F. Software update: the ORCA program system, version 4.0. *WIREs Comput. Mol. Sci.* **2018**, *8*, e1327.
(27) Grimme, S.; Antony, J.; Ehrlich, S.; Krieg, H. A consistent and accurate ab initio parametrization of density functional dispersion correction (DFT-D) for the 94 elements H-Pu. *J. Chem. Phys.* **2010**, *132*, 154104.
(28) Grimme, S.; Ehrlich, S.; Goerigk, L. Effect of the damping function in dispersion corrected density functional theory. *J. Comput. Chem.* **2011**, *32*, 1456–1465.
(29) Grimme, S. Semiempirical hybrid density functional with perturbative second-order correlation. *J. Chem. Phys.* **2006**, *124*, 034108.
(30) Lindner, E.; Auch, K.; Hiller, W.; Fawzi, R. Methyl(thioxo)phosphane: Generation and Trapping Reaction with $Mn_2(CO)_{10}$. *Angew. Chem. Int. Ed. Engl.* **1984**, *23*, 320–320.
(31) Hussong, R.; Heydt, H.; Maas, G.; Regitz, M. Über die Abfangreaktion von Phenylthioxophosphan mit Hexacarbonylbis(cyclopentadienyl)dimolybdän. *Chem. Ber.* **1987**, *120*, 1263–1267.
(32) Bohle, D. S.; Rickard, C. E. F.; Roper, W. R. [Os(η^2-PHS)$(CO)_2(PPh_3)_2$], a Stable η^2-Thioxophosphane(H–P=S)-Metal Complex. *Angew. Chem. Int. Ed. Engl.* **1988**, *27*, 302–304.
(33) Lorenz, I.-P.; Mürschel, P.; Pohl, W.; Polborn, K. Mono- und Diferriophosphane und -thioxophosphorane. *Chem. Ber.* **1995**, *128*, 413–416.
(34) Alvarez, C. M.; Alvarez, M. A.; García, M. E.; González, R.; Ruiz, M. A.; Hamidov, H.; Jeffery, J. C. High-Yield Synthesis and Reactivity of Stable Diiron Complexes with Bent-Phosphinidene Bridges. *Organometallics* **2005**, *24*, 5503–5505.
(35) Weng, Z.; Leong, W. K.; Vittal, J. J.; Goh, L. Y. Complexes from Ring Opening of Lawesson's Reagent and Phosphorus-Phosphorus Coupling. *Organometallics* **2003**, *22*, 1645–1656.
(36) Chai, J.; Tian, R.; Wu, D.; Wei, D.; Xu, Q.; Duan, Z.; Mathey, F. The coordination chemistry of phosphinidene sulfides. Synthesis and catalytic properties of Pd4 and Pt4 clusters. *Dalton Trans.* **2018**, ASAP.
(37) Pyykkö, P.; Atsumi, M. Molecular Double-Bond Covalent Radii for Elements Li–E112. *Chem. Eur. J.* **2009**, *15*, 12770–12779.
(38) Glendening, E. D.; Badenhoop, J. K.; Reed, A. E.; Carpenter, J. E.; Bohmann, J. A.; Morales, C. M.; Landis, C. R.; Weinhold, F. NBO 6.0 (Theoretical Chemistry Institute, University of Wisconsin, Madison, 2013).
(39) Nakayama, S.; Yoshifuji, M.; Okazaki, R.; Inamoto, N. Reactions of Phosphinothioylidenes with cis- and trans-Stilbene Oxides. *Bull. Chem. Soc. Jpn.* **1975**, *48*, 3733–3737.
(40) Holand, S.; Mathey, F. New method for building carbon-phosphorus heterocycles. *J. Org. Chem.* **1981**, *46*, 4386–4389.
(41) Tomioka, H.; Miura, S.; Izawa, Y. Synthesis and photochemical reaction of diels-alder adduct of phosphole oxide and cyclopentadiene. *Tetrahedron Letters* **1983**, *24*, 3353–3356.
(42) Wong, T.; Terlouw, J. K.; Keck, H.; Kuchen, W.; Tommes, P. The thioxophosphane H–P=S and its tautomer H–S–P, (thiohydroxy)phosphinidene, are stable in the gas phase. *J. Am. Chem. Soc.* **1992**, *114*, 8208–8210.
(43) MacKay, D. D. S.; Charnley, S. B. Phosphorus in circumstellar envelopes. *Mon. Not. R. Astron. Soc.* **2001**, *325*, 545–549.
(44) Halfen, D. T.; Clouthier, D. J.; Ziurys, L. M.; Lattanzi, V.; McCarthy, M. C.; Thaddeus, P.; Thorwirth, S. *J. Chem. Phys.* **2011**, *134*, 134302.
(45) Grimminger, R.; Clouthier, D. J.; Tarroni, R.; Wang, Z.; Sears, T. J. An experimental and theoretical study of the electronic spectrum of HPS, a second row HNO analog. *J. Chem. Phys.* **2013**, *139*, 174306.
(46) Heydt, H.; Ehle, M.; Haber, S.; Hoffmann, J.; Wagner, O.; Göller, A.; Clark, T.; Regitz, M. Reactions of 1-Chloro-1*H*-phosphirenes with Nucleophiles. *Chem. Ber.* **1997**, *130*, 711–723.
(47) Sweeney, J. B. 40.1.5.2.1 Ring Opening of Saturated Aziridines. *Science of Synthesis* **2009**, *40*, 712.
(48) Niecke, E.; Leuer, M.; Nieger, M. Synthese und Reaktivität eines 1-Chlor-λ^3-phosphirans. *Chem. Ber.* **1989**, *122*, 453–461.
(49) Lagrone, C. B.; Schauer, S. J.; Thomas, C. J.; Gray, G. M.; Watkins, C. L.; Krannich, L. K. Reactivity of R_2AlH (R = Me, Bu-*i*) with Selected Aminoarsines and Secondary Amines. *Organometallics* **1996**, *15*, 3980–3984.
(50) Benkő, Z.; Streubel, R.; Nyulászi, L. Stability of phosphinidenes—Are they synthetically accessible? *Dalton Trans.* **2006**, *0*, 4321–4327.
(51) Yaghlane, S. B.; Cotton, C. E.; Francisco, J. S.; Linguerri, R.; Hochlaf, M. Ab initio structural and spectroscopic study of HPS_x and HSP_x (x = 0,+1,-1) in the gas phase. *J. Chem. Phys.* **2013**, *139*, 174313.
(52) Johansson, S.; Kuhlmann, C.; Weber, J.; Paululat, T.; Engelhard, C.; Günne, J. S. a. d. Decomposition of P_4O_{10} in DMSO. *Chem. Commun.* **2018**, *54*, 7605–7608.
(53) Mielke, Z.; Brabson, G. D.; Andrews, L. Matrix infrared spectra of the phosphorus sulfides PS, P_2S and PS_2. *J. Phys. Chem.* **1991**, *95*, 75–79.
(54) Bews, J. R.; Glidewell, C. Structures and Energies of Mass Spectral Fragments Derived from Phosphorus Trisulphide. *J. Mol. Struct. THEOCHEM* **1982**, *86*, 217–230.
(55) Our calculations predict the gas phase reaction 2 HPS → H_2S + P_2S to be downhill (ΔH = –13.1 kcal/mol, ΔS = –4.1 cal/mol·K) at the RI-B2PLYP-D3(BJ)/Def2-TZVP level of theory.
(56) Schlesinger, M. E. The Thermodynamic Properties of Phosphorus and Solid Binary Phosphides. *Chem. Rev.* **2002**, *102*, 4267–4302.
(57) Boulouch, R. Sur les mixtes formés par le soufre et le phosphore au-dessous de 100°. *Compt. Rend.* **1902**, *135*, 165–168.
(58) Monteil, Y.; Vincent, H. Système ternaire phosphore rouge-soufre-sélénium II. Diagramme polythermique. *Bull. Soc. Chim. Fr., Partie 1* **1975**, 1029–1033.
(59) Blachnik, R.; Hoppe, A. Präparation und thermochemische Untersuchung von Verbindungen der Systeme Phosphor-Schwefel und Phosphor-Selen. *Z. Anorg. Allg. Chem.* **1979**, *457*, 91–104.
(60) Okamoto, H. P-S (Phosphorus-sulfur). *J. Phase Equilib.* **1991**, *12*, 706–707.
(61) Schneider, A.; Förthmann, R. Process for the manufacture of tetraphosphorus disulfide. US3387936A, 1968.
(62) Monteil, Y.; Vincent, H. Phosphorus Compounds with the VI B Group Elements. *Z. Naturforsch. B* **1976**, *31*, 668–672.
(63) Sanchez, M.; Wolf, R.; Mathis, F. Intensité d'absorption de la vibration de valence P–H dans des composés organiques du phosphore: XYP(=O)H et XYP(=S)H. *Spectrochim. Acta A* **1967**, *23*, 2617–2630.
(64) Lin-Vien, D.; Colthup, N. B.; Fateley, W. G.; Grasselli, J. G.

The Handbook of Infrared and Raman Characteristic Frequencies of Organic Molecules; Academic Press: Boston, 1991.
(65) Zingaro, R. A. Phosphine Sulfides and Selenides: The Phosphorus-Sulfur and Phosphorus-Selenium Stretching Frequencies. *Inorg. Chem.* **1963**, *2*, 192–196.
(66) Burns, G. R.; Rollo, J. R.; Syme, R. W. G. Raman spectra of single crystals of α-P_4S_3. *J. Raman Spectrosc.* **1988**, *19*, 345–351.
(67) Olego, D. J.; Baumann, J. A.; Kuck, M. A.; Schachter, R.; Michel, C. G.; Raccah, P. M. The microscopic structure of bulk amorphous red phosphorus: A Raman scattering investigation. *Solid State Commun.* **1984**, *52*, 311–314.
(68) Koudelka, L.; Pisárčik, M.; Gutenev, M. S.; Blinov, L. N. Raman spectra and short-range order in P_xS_{1-x} glasses. *J. Mater. Sci. Lett.* **1989**, *8*, 933–934.
(69) Eckert, H.; Liang, C. S.; Stucky, G. D. Phosphorus-31 magic angle spinning NMR of crystalline phosphorus sulfides: correlation of phosphorus-31 chemical shielding tensors with local environments. *J. Phys. Chem.* **1989**, *93*, 452–457.
(70) Bytchkov, A.; Fayon, F.; Massiot, D.; Hennet, L.; Price, D. L. ^{31}P solid-state NMR studies of the short-range order in phosphorus–selenium glasses. *Phys. Chem. Chem. Phys.* **2010**, *12*, 1535–1542.
(71) Harris, R. K.; Wilkes, P. J.; Wood, P. T.; Woollins, J. D. Solid-state phosphorus-31 nuclear magnetic resonance spectroscopy of phosphorus sulphides. *J. Chem. Soc., Dalton Trans.* **1989**, *0*, 809–813.
(72) Lathrop, D.; Eckert, H. Chemical disorder in non-oxide chalcogenide glasses. Site speciation in the system phosphorus-selenium by magic angle spinning NMR at very high spinning speeds. *J. Phys. Chem.* **1989**, *93*, 7895–7902.
(73) Tullius, M.; Lathrop, D.; Eckert, H. Glasses in the system phosphorus-sulfur: a phosphorus-31 spin-echo and high-speed MAS-NMR study of atomic distribution and local order. *J. Phys. Chem.* **1990**, *94*, 2145–2150.
(74) Gibby, M. G.; Pines, A.; Rhim, W.-K.; Waugh, J. S. ^{31}P Chemical Shielding Anisotropy in Solids. Single Crystal and Powder Studies at 99.4 MHz. *J. Chem. Phys.* **1972**, *56*, 991–995.
(75) Pelavin, M.; Hendrickson, D. N.; Hollander, J. M.; Jolly, W. L. Phosphorus 2*p* electron binding energies. Correlation with extended Hueckel charges. *J. Phys. Chem.* **1970**, *74*, 1116–1121.
(76) Klimov, V. D.; Vashman, A. A.; Pronin, I. S. Reaction of Atomic Titanium with a PF_3 Matrix at 77 K: Cryochemical Synthesis of the Novel Compound $TiF_2{\cdot}PF_3$. *Zh. Obshch. Khim.* **1991**, *61*, 2166.
(77) A small feature at higher binding energy (134.4 eV) was likely due to air exposure upon sample loading.
(78) Peisert, H.; Chassé, T.; Streubel, P.; Meisel, A.; Szargan, R. Relaxation energies in XPS and XAES of solid sulfur compounds. *J. Electron Spectrosc. Relat. Phenom.* **1994**, *68*, 321–328.
(79) Küper, G.; Hormes, J.; Sommer, K. In situ X-ray absorption spectroscopy at the K-edge of red phosphorus in polyamide 6,6 during a thermo-oxidative degradation. *Macromol. Chem. Phys.* **1994**, *195*, 1741–1753.
(80) Bose, M.; Root, R. A.; Pizzarello, S. A XANES and Raman investigation of sulfur speciation and structural order in Murchison and Allende meteorites. *Meteorit. Planet. Sci.* **2017**, *52*, 546–559.
(81) Raabe, I.; Antonijevic, S.; Krossing, I. Dynamics and Counterion-Dependence of the Structures of Weakly Bound Ag^+–P_4S_3 Complexes. *Chem. Eur. J.* **2007**, *13*, 7510–7522.
(82) Thurn, H.; Krebs, H. Über Struktur und Eigenschaften der Halbmetalle. XXII. Die Kristallstruktur des Hittorfschen Phosphors. *Acta Cryst. B* **1969**, *25*, 125–135.
(83) Proffen, T.; Billinge, S. J. L.; Egami, T.; Louca, D. Structural analysis of complex materials using the atomic pair distribution function — a practical guide. *Z. Kristallogr.* **2003**, *218*, 132–143.
(84) Ruck, M. Darstellung und Kristallstruktur des ersten polymeren Phosphorselenids catena-$(P_4Se_4)_x$. *Z. Anorg. Allg. Chem.* **1994**, *620*, 1832–1836.
(85) Verrall, D. J.; Gladden, L. F.; Elliott, S. R. The Structure of Phosphorus Selenide Glasses. *J. Non-Cryst. Solids* **1988**, *106*, 47–49.
(86) Verrall, D. J.; Elliott, S. R. Structure of Phosphorus Selenide Glasses. *J. Non-Cryst. Solids* **1989**, *114*, 34–36.
(87) Verrall, D. J.; Elliott, S. R. *Neutron and X-Ray Scattering: Complementary Techniques*; Institute of Physics Conference Series; IOP Publishing Ltd.: Canterbury, England, 1990; Vol. 101; pp 87–95.
(88) Phillips, R. T.; Wolverson, D.; Burdis, M. S.; Fang, Y. Observation of discrete molecular structures in glassy P_xSe_{1-x} by Raman spectroscopy. *Phys. Rev. Lett.* **1989**, *63*, 2574–2577.
(89) Sergi, A.; Ferrario, M.; Buda, F.; McDonald, I. R. First-principles simulation of phosphorus-selenium systems. *Chem. Phys. Lett.* **1996**, *259*, 301–306.
(90) Sergi, A.; Ferrario, M.; Buda, F.; McDonald, I. R. Structure of phosphorus-selenium glasses: results from ab initio molecular dynamics simulations. *Mol. Phys.* **2000**, *98*, 701–707.
(91) Morigaki, K.; Kugler, S.; Shimakawa, K. *Amorphous Semiconductors*; Materials for Electronic and Optoelectronic Applications; Wiley-Blackwell: West Sussex, UK, 2017; pp 157–229.
(92) Madelung, O. *Semiconductors: Data Handbook*; Springer, Berlin, Heidelberg, 2004; pp 613–633.
(93) Shida, N.; Buss, J. A.; Agapie, T. Mild electrochemical synthesis of metal phosphides with dibenzo-7-phosphanorbornadiene derivatives: mechanistic insights and application to proton reduction in water. *Chem. Commun.* **2018**, *54*, 767–770.
(94) Hu, Z.; Yuan, L.; Liu, Z.; Shen, Z.; Yu, J. C. An Elemental Phosphorus Photocatalyst with a Record High Hydrogen Evolution Efficiency. *Angew. Chem. Int. Ed.* **2016**, *55*, 9580–9585.